Shear instability in twisted bilayer graphene

Xianqing Lin,[1,2] Dan Liu,[1] and David Tománek[1,*]
[1]*Physics and Astronomy Department, Michigan State University, East Lansing, Michigan 48824, USA*
[2]*College of Science, Zhejiang University of Technology, Hangzhou 310023, China*

(Received 1 September 2018; published 21 November 2018)

In twisted bilayer graphene (TBLG), extremely small deviations from the magic twist angle $\theta_m \approx 1.08^\circ$ change its electronic structure near the Fermi level drastically, causing a meV-wide flat band to appear or disappear. In view of such sensitivity to minute structural deformations, we investigate the combined effect of shear and atomic relaxation on the electronic structure. Using precise experimental data for monolayer and bilayer graphene as input in a simplified formalism for the electronic structure and elastic energy, we find TBLG near θ_m to be unstable with respect to global shear by the angle $\alpha \approx 0.08^\circ$. In TBLG, the effect of shear on the electronic structure is as important as that of atomic relaxation. Under optimum global shear, calculated θ_m is reduced by 0.04° and agrees with the observed value.

DOI: 10.1103/PhysRevB.98.195432

I. INTRODUCTION

Theoretically postulated [1–4] drastic changes in the electronic structure at the Fermi level E_F of bilayer graphene (BLG) near the "magic" twist angle $\theta_m \approx 1.08^\circ$ were recently confirmed experimentally [5,6] and ignited a feverish research effort in twisted BLG (TBLG). Superconductivity [6] and strongly correlated electronic behavior [5], observed at θ_m, are associated with a meV-wide flat band around the Dirac point [1] at E_F with a vanishing density of states (DOS). This flat band, which is formed only within an extremely narrow range $\Delta\theta < 0.1^\circ$ around θ_m, is separated by band gaps above and below from the rest of the electronic spectrum [1,5–7]. From the viewpoint of atomic structure, nonzero twist causes a moiré pattern with domains of AB, BA, and AA stacking to change rapidly in size, especially at small values of the twist angle θ. In view of the unusual sensitivity of the electronic structure to twist angle θ alone, we study here the effect of two other soft deformation modes, namely, global shear and atomic relaxation in TBLG. Published data suggest that shear does affect the electronic structure of untwisted and unrelaxed BLG [8] but do not report associated energy changes. Many calculations have explored atomic relaxations in untwisted [9] and twisted BLG and their effect on the electronic structure [10–18] but have ignored inhomogeneities in the stacking structure observed by high-resolution transmission electron microscopy (TEM) [19,20].

Here we combine continuum elasticity theory with a tight-binding description of the electronic structure [21] to study the behavior of BLG under combined twist and shear. We focus on geometries with a twist angle θ near the observed magic angle $\theta_m \approx 1.08^\circ$, where the electronic structure, including the appearance and disappearance of a flat band near E_F as well as band gaps above and below, shows extreme sensitivity to structural deformations. We find TBLG near θ_m to be energetically unstable with respect to global shear by the angle $\alpha \approx 0.08^\circ$. Also, we find that the effect of shear on the electronic structure is as important as that of atomic relaxation. Under optimum global shear, calculated θ_m is reduced by 0.04° and agrees with the observed value.

II. COMPUTATIONAL APPROACH

We use precise experimental data for monolayer and bilayer graphene as input for our calculations. For unstable geometries, where such data are not available, we use *ab initio* density functional theory (DFT) as implemented in the VASP code [22–24]. We used projector augmented-wave pseudopotentials [25,26] and the SCAN+rVV10 exchange-correlation functional [27], which provides a proper description of the van der Waals interaction [27,28]. We used 800 eV as the electronic kinetic energy cutoff for the plane-wave basis and a total energy difference between subsequent self-consistency iterations below 10^{-5} eV/atom as the criterion for self-consistency. We reached full convergence since our calculations were limited to very small unit cells of AA- and AB-stacked BLG.

III. RESULTS

A. Deformation modes in bilayer graphene

The softest deformation modes of BLG are relative translation and rotation of the constituent graphene layers. BLG subject to uniform twist creates a moiré lattice of equilateral triangles, and rigid displacement only translates this lattice with no effect on the atomic and electronic structure. Atomic relaxations including local bending in TBLG, as well as global shear and stretch of the monolayers, require more energy. Global stretch, which involves bond stretching, is energetically harder than global shear, which involves only bond bending. Global shear creates a stripe pattern of domains [8]. The combination of twist and shear has not been explored so far.

The deformation of BLG under shear and twist is defined in Fig. 1(a). In the initially AA-stacked BLG, we define the shear direction within the top layer by the angle β with respect to the armchair direction. After first being sheared by the

*tomanek@pa.msu.edu

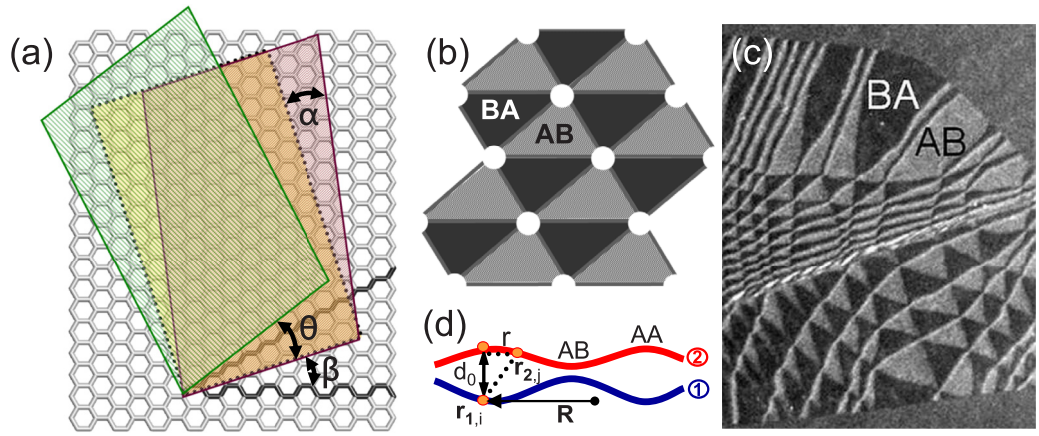

FIG. 1. Shear and twist in BLG. (a) Definition of shear and twist operations in BLG, initially a bilayer in AA stacking indicated by the honeycomb lattice. A rectangular segment of the top layer, with one side closing the angle β with respect to the highlighted armchair direction, is indicated in yellow and surrounded by the dotted line. The segment is first sheared by the angle α and subsequently rotated by the angle θ. (b) Schematic top view of a uniformly twisted and sheared monolayer graphene (MLG) on top of an undeformed MLG. The resulting relaxed moiré pattern contains regions of AA stacking, highlighted by the white circles, and those of AB or BA stacking. (c) Dark-field TEM image of bilayer graphene reproduced from Ref. [19]. (d) Schematic side view of a relaxed sheared and twisted BLG with locally varying stacking.

angle α, the top layer is subsequently rotated by the angle θ. The mathematical formulation of the shear-twist deformation in BLG is detailed in the Appendix. The general moiré pattern of a sheared and twisted BLG is lattice asymmetric triangles with AA-stacked regions forming the vertices, as shown schematically in Fig. 1(b). The triangular regions of AB and BA stacking between the vertices have no symmetry in general but become equilateral in the case of pure twist in the BLG associated with $\alpha = 0^\circ$. Figure 1(c) contains a reproduction of a dark-field TEM image of the BLG reported in Ref. [19]. The triangular lattice in Fig. 1(c) is strongly distorted due to inhomogeneous twist and strain. Quantities associated with atomic relaxation are defined in the schematic side view of sheared and twisted BLG in Fig. 1(d). The local interlayer distance d_0 depends on the two-dimensional (2D) position vector $\mathbf{R}$ within the BLG plane, which distinguishes regions with different local stacking sequences.

B. Relaxations in sheared and twisted bilayer graphene

To quantify the effect of relaxation in the BLG, we consider both in-plane and out-of-plane deformations and calculate changes in the total energy $E_{\rm tot} = E_{el} + E_{\rm int}$ in terms of the elastic deformation energy E_{el} of the individual layers and the interlayer interaction energy $E_{\rm int}$. The displacement of atom i at $\mathbf{r}_{n,i}$, defined in Fig. 1(d) for layers $n = 1, 2$, is described by a continuous displacement field with an in-plane component $\mathbf{u}^{(n)}(\mathbf{R})$ and an out-of-plane component $h^{(n)}(\mathbf{R})$. The elastic deformation energy is given by [29]

$$E_{el} = \sum_{n=1}^{2} \int d\mathbf{R} \Bigg\{ \frac{\kappa}{2} \left(\frac{\partial^2 h^{(n)}}{\partial x^2} + \frac{\partial^2 h^{(n)}}{\partial y^2} \right)^2 + \frac{\lambda+\mu}{2} \left(\frac{\partial u_x^{(n)}}{\partial x} + \frac{\partial u_y^{(n)}}{\partial y} \right)^2 + \frac{\mu}{2} \left[\left(\frac{\partial u_x^{(n)}}{\partial x} - \frac{\partial u_y^{(n)}}{\partial y} \right)^2 + \left(\frac{\partial u_y^{(n)}}{\partial x} + \frac{\partial u_x^{(n)}}{\partial y} \right)^2 \right] \Bigg\}, \quad (1)$$

where the integral extends over the moiré pattern supercell. We use $\kappa = 1.4\,\text{eV}$ for the flexural rigidity [30] and $\lambda = 4.23\,\text{eV/Å}^2$ and $\mu = 9.04\,\text{eV/Å}^2$ for the 2D elastic Lamé factors [18] of graphene.

To calculate the interlayer interaction energy $E_{\rm int}$, we first characterize the local stacking at position $\mathbf{R} = \mathbf{r}_{1,i}$ of atom i in layer 1, shown in Fig. 1(d), by calculating the connection vectors $\mathbf{r}_{2,j} - \mathbf{r}_{1,i}$ to all atoms j of the same sublattice in layer 2 and their projections onto the x-y plane of the lattice. The shortest among these vectors is then called the shift vector [9] $\boldsymbol{\delta}(\mathbf{R})$. With this definition, $|\boldsymbol{\delta}| = 0$ in AA-stacked BLG, and $|\boldsymbol{\delta}| = a/\sqrt{3}$ in AB-stacked BLG, where $a = 2.46$ Å is the lattice constant of graphene. The observed interlayer distance in the stable AB-stacked BLG is $d_0^{AB} = 3.35$ Å. The corresponding calculated value for AA-stacked BLG, which is less stable by $\Delta E = 0.38\,\text{eV/nm}^2$, is $d_0^{AA} = 3.60$ Å.

The interlayer interaction energy depends on the local interlayer separation $d_0(\mathbf{R})$ and the local shift vector $\boldsymbol{\delta}(\mathbf{R})$. Since the moiré supercells are much larger than the interatomic distance in the twist angle range of interest, both quantities can be represented well by a continuous field. Then, the interlayer interaction energy is given by the integral

$$E_{\rm int} = \int V(\mathbf{R}) d\mathbf{R}, \quad (2)$$

which extends over the moiré supercell. We represent the interlayer interaction potential $V(\mathbf{R}) = V[\boldsymbol{\delta}(\mathbf{R}), d_0(\mathbf{R})]$, as well as the quantities d_0 and $\boldsymbol{\delta}$, by a Fourier expansion over the BLG lattice [11], which is detailed in the Appendix. The expansion requires only a few of the shortest reciprocal superlattice vectors of the BLG and is trivial for an untwisted BLG with AA and AB stackings, where $V = \text{const}$ and $V^{AA} - V^{AB} = 0.38\,\text{eV/nm}^2$.

The optimum geometry of the relaxed BLG that had been subject to global shear and twist is obtained by globally minimizing the total energy, which has been determined using a Fourier expansion detailed in the Appendix.

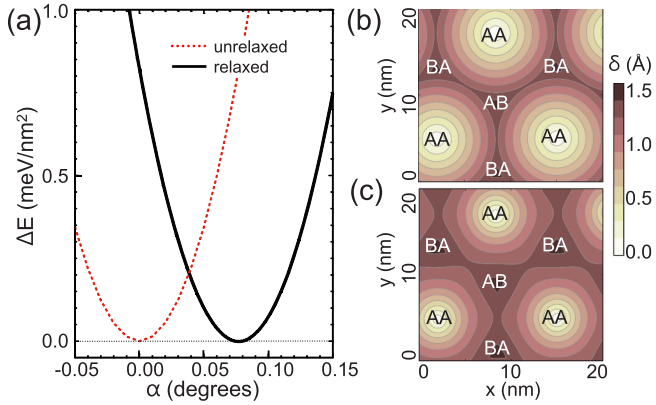

FIG. 2. (a) Energy difference ΔE caused by shearing the top layer of BLG, which had been twisted by $\theta_m = 1.08^\circ$, by varying the shear angle α along the $\beta = 0^\circ$ direction. Results for the BLG with unrelaxed atomic positions in planar, sheared monolayers are shown by the red dotted line and for the BLG with relaxed atomic positions by the black solid line. Contour plots of the local shift vector length $\delta = |\boldsymbol{\delta}|$ in the BLG structure, which had been twisted by $\theta_m = 1.08^\circ$ and sheared by $\alpha = 0.08^\circ$ along the $\beta = 0^\circ$ direction, (b) in the absence and (c) in the presence of lattice relaxation.

Whereas lattice relaxation is driven by energy gain, shear distortion of a monolayer requires energy investment. For a given twist angle θ, it is conceivable that the energy invested in shear may be outweighed by an additional energy gain associated with relaxation to a more favorable structure. This situation is illustrated in Fig. 2(a), which shows energy changes in TBLG with $\theta_m = 1.08^\circ$. We found the energy values, which are shown for shear along the $\beta = 0^\circ$ direction, to be nearly identical for shear along $\beta = 30^\circ$, and conclude that the shear energy does not depend on β. When lattice relaxation is suppressed, as shown by the dotted line, the stablest geometry is unsheared with $\alpha = 0^\circ$. When allowing for lattice relaxation, the optimum geometry has acquired a global shear angle $\alpha = 0.08^\circ$.

The absolute value of the local shift vector $\delta = |\boldsymbol{\delta}|$ as a function of $\mathbf{R} = (x, y)$ is shown in Figs. 2(b) and 2(c) for BLG structures that have been twisted by $\theta_m = 1.08^\circ$ and sheared by the small angle $\alpha = 0.08^\circ$ along the $\beta = 0^\circ$ direction. The corners of the moiré supercell, shown in white, are the unshifted AA regions with $\delta = 0$. In the unrelaxed structure of Fig. 2(b), the energetically favorable regions of AB or BA stacking are rather small. Upon relaxation, these favorable stacking regions increase in size, as seen in Fig. 2(c). The effect of relaxation becomes much more visible at smaller twist angles θ associated with very large moiré domains. As seen in Fig. 4, the AB and BA domains then acquire a distinctly triangular shape upon relaxation, which has been observed in TEM images [19,20], including Fig. 1(c).

C. Electronic structure of sheared, twisted, and relaxed bilayer graphene

To study the combined effect of shear, twist, and atomic relaxation on the electronic structure of BLG, we use an extension of the minimum Hamiltonian [21] that had successfully reproduced the electronic structure of twisted BLG. Due to the high in-plane stiffness and flexural rigidity of graphene, the atomic relaxation is rather small and smooth across the BLG lattice, so that the intralayer nearest-neighbor Hamiltonian with $V^0_{pp\pi} = 3.09\,\text{eV}$ is not affected. Since the interlayer separation changes between the values d_0^{AA} and d_0^{AB} within each moiré domain, as seen in Fig. 1(d), we modify the expressions for the interlayer hopping in Ref. [21] to

$$t(r, \mathbf{R}) = V^0_{pp\sigma}(d_0) e^{-(\sqrt{r^2+d_0^2}-d_0)/\lambda} \frac{d_0^2}{r^2+d_0^2}, \tag{3}$$

where

$$V^0_{pp\sigma}(d_0) = V^0_{pp\sigma}\left(d_0^{AB}\right) e^{-(d_0-d_0^{AB})/\lambda'}. \tag{4}$$

In these expressions, the only quantity that depends on the position $\mathbf{R}$ within the layer is the local interlayer separation $d_0 = d_0(\mathbf{R})$, defined in Fig. 1(d). For the unrelaxed geometry with $d_0 = d_0^{AB} = \text{const}$, the values $V^0_{pp\sigma}(d_0^{AB}) = 0.39\,\text{eV}$, $d_0^{AB} = 3.35\,\text{Å}$, $\lambda = 0.27\,\text{Å}$ were established in Ref. [21]. We furthermore use the parameter $\lambda' = 0.58\,\text{Å}$ to adequately describe the dependence of $V^0_{pp\sigma}$ on the interlayer separation to match our DFT calculations.

In TBLG, where atomic relaxation was not considered explicitly in a related previous study [21], we determined the electronic structure at the interlayer distance d_0^{AB} using the same continuum method for the description of eigenstates. In unrelaxed TBLG subject to shear, the interlayer Hamilton matrix elements of Ref. [21] are modified as

$$\langle \psi_{1,\eta}(\mathbf{k_1}) | H | \psi_{2,\xi}(\mathbf{k_2}) \rangle = \sum_{\mathbf{G},\mathbf{G}'} \frac{\tilde{t}(|\mathbf{k_1}+\mathbf{G}|)}{\Omega} e^{i(\mathbf{G}\cdot\boldsymbol{\tau}_\eta - \mathbf{G}'\cdot\boldsymbol{\tau}'_\xi)} \delta_{\mathbf{k_2}-\mathbf{k_1},\mathbf{G}-\mathbf{G}'}. \tag{5}$$

Here we use η and ξ to represent the two sublattices with the basis vectors $\boldsymbol{\tau}$ in the unsheared bottom layer 1 and $\boldsymbol{\tau}'$ in the top layer 2 that has been sheared and twisted. $\mathbf{k_n}$ is the momentum vector in layer n. $\tilde{t}(k)$ is the 2D Fourier transform of $t(r)$ that is independent of the position within the unrelaxed bilayer, which is kept at the constant optimum interlayer separation d_0^{AB}. $\mathbf{G}$ is the reciprocal lattice vector of the bottom layer 1, and $\mathbf{G}'$ is the reciprocal lattice vector of the sheared and twisted top layer 2. For nonspecific values of α, β, and θ, the BLG lattice is generally incommensurate but can be approximated by a commensurate moiré superlattice with large unit cells.

For small twist angles, the reciprocal lattice vectors of the undeformed bottom layer 1 in Eq. (5) can be approximated by $\mathbf{G} = n_1\mathbf{b}_1 + n_2\mathbf{b}_2$, and those of the deformed top layer 2 can be approximated by $\mathbf{G}' = n_1\mathbf{b}'_1 + n_2\mathbf{b}'_2$, with n_1 and n_2 being small integers. In these expressions, $\mathbf{b}_{1/2}$ are the two vectors spanning the reciprocal lattice of the bottom layer, and $\mathbf{b}'_{1/2}$ are those spanning the reciprocal lattice of the deformed top layer. In relaxed commensurate BLG structures, we do not use Eq. (5), but rather diagonalize the tight-binding Hamiltonian directly to obtain the electronic band structure.

The effect of shear and atomic relaxation on the DOS of TBLG subject to twist by the magic angle $\theta_m = 1.08^\circ$ is discussed in Fig. 3 for energies close to E_F and in Fig. 5 for a wider energy range. The DOS characteristics at θ_m are a narrow "flat band" around the Dirac point with vanishing DOS

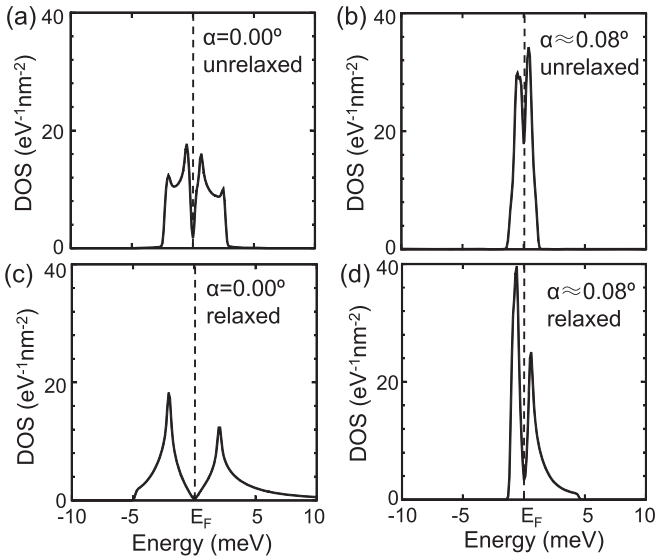

FIG. 3. Electronic density of states (DOS) in the BLG structure subject to the magic twist angle $\theta_m = 1.08^\circ$. Results for the unsheared structure are shown in (a) and (c), and those for the top layer sheared by $\alpha = 0.08^\circ$ along the $\beta = 0^\circ$ direction are shown in (b) and (d). Results for the unrelaxed structure in (a) and (b) are compared to those for the relaxed structure in (c) and (d).

at E_F and band gaps above and below. The DOS of unsheared and unrelaxed TBLG in Fig. 3(a) is the same as in a previous report [21] for the same structure, where shear and atomic relaxation were not considered explicitly. Subjecting BLG to global shear by $\alpha = 0.08^\circ$ while suppressing any atomic relaxation reduces the width of the flat significantly, as seen in Fig. 3(b), to almost half its value in unsheared TBLG. This result alone proves that even minor shear plays a significant role in the electronic structure of TBLG. As seen in Fig. 3(c), atomic relaxation alone increases the width of the band near E_F significantly with respect to the structure in Fig. 3(a) to the degree that the designation "flat band" is no longer appropriate. Subjecting this relaxed structure to minor shear of $\alpha = 0.08^\circ$, however, narrows down this band to resemble that in Fig. 3(a) for TBLG irrespective of shear and relaxation. Thus, taking shear into account is essential to properly identify the θ_m value in relaxed TBLG. We compared the widths of the narrow band around E_F for unsheared and sheared TBLG with atomic relaxation. Our results, reproduced in Fig. 6, suggest that the minimum bandwidth is found at the magic angle $\theta_m = 1.12^\circ$ in relaxed TBLG with suppressed shear. This value is larger than the magic angle value $\theta_m = 1.08^\circ$ that is observed in sheared and relaxed TBLG.

IV. DISCUSSION

As reported in the discussion of shear in Fig. 2(a), the deformation energy ΔE is nearly independent of the shear direction β. Nevertheless, β modifies strongly the shape of the triangles in the moiré superlattice. Local changes in the shear angle α and direction β are clearly visible in the TEM images of BLG reported in Fig. 1(c) and Refs. [19,20]. We also note that the high-energy cost of in-layer deformations including shear limits the degree of atomic relaxation. Distributing shear from one to both layers of BLG should cut this energy cost in half in the harmonic regime, thus reducing the limits imposed on atomic relaxation and providing extra energy gain for the system.

V. SUMMARY AND CONCLUSIONS

In conclusion, we studied the effect of combined shear and twist on the energy as well as the atomic and electronic structure of BLG. We found that the observed drastic changes in the electronic structure near the Fermi level, caused by minute changes in the twist angle away from the magic value $\theta_m \approx 1.08^\circ$, are strongly affected by lattice relaxation and global shear. Using precise experimental data for monolayer and bilayer graphene as input in a simplified formalism for the electronic structure and elastic energy, we found TBLG near θ_m to be unstable with respect to global shear by the angle $\alpha \approx 0.08^\circ$. We also found that shear and atomic relaxation modified the electronic structure of TBLG to a similar degree. At optimum global shear, the calculated value of the magic angle θ_m in relaxed TBLG is reduced by 0.04° to agree with the observed value of 1.08°.

ACKNOWLEDGMENTS

D.T. and D.L. acknowledge financial support from NSF/AFOSR EFRI 2-DARE Grant No. EFMA-1433459. X.L. acknowledges support from the China Scholarship Council. Computational resources were provided by the Michigan State University High Performance Computing Center.

APPENDIX

1. Mathematical formulation of the rigid shear-twist deformation in bilayer graphene

Before describing the shear-twist deformation in bilayer graphene (BLG), we need to recall that the honeycomb lattice of graphene consists of two triangular sublattices, A and B. The Bravais lattice of the bottom layer 1 is spanned by the vectors $\mathbf{a_1} = a(\sqrt{3}/2, -1/2)$ and $\mathbf{a_2} = a(\sqrt{3}/2, 1/2)$ in Cartesian coordinates, where $a = 2.46$ Å is the lattice constant of graphene. The basis vectors of the sublattices are $\boldsymbol{\tau}_A = 0$ and $\boldsymbol{\tau}_B = (\mathbf{a_1} + \mathbf{a_2})/3$. Initially, the top layer 2 of the BLG is on top of layer 1 in AA stacking.

The sheer-twist transformation of the BLG top layer with respect to the bottom layer is shown schematically in Fig. 1(a). Pure shear in the graphene top layer by the angle α along the shear direction angle β with respect to the armchair direction is described by the transformation matrix

$$S_\alpha = \begin{pmatrix} 1 - \sin\beta\cos\beta\tan\alpha & (\cos\beta)^2\tan\alpha \\ -(\sin\beta)^2\tan\alpha & 1 + \sin\beta\cos\beta\tan\alpha \end{pmatrix}. \quad \text{(A1)}$$

A pure counterclockwise twist of the top layer by the angle θ with respect to the bottom layer is described by the unitary transformation matrix

$$T_\theta = \begin{pmatrix} \cos\theta & -\sin\theta \\ \sin\theta & \cos\theta \end{pmatrix}. \quad \text{(A2)}$$

The shear-twist operation transforms the two Bravais lattice vectors $\mathbf{a_j}$ of the top layer to $\mathbf{a'_j} = T_\theta S_\alpha \mathbf{a_j}$, with $j = 1, 2$. Ex-

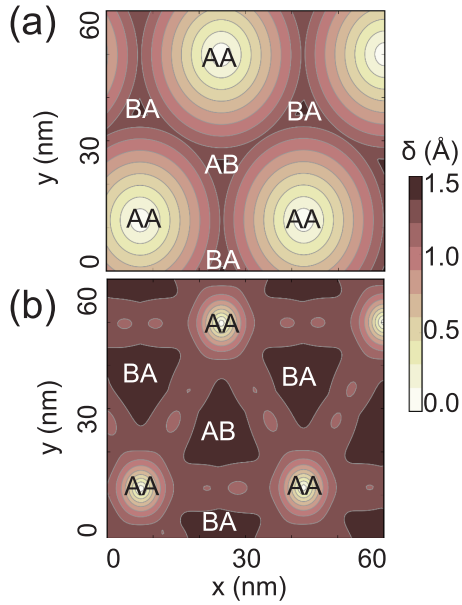

FIG. 4. Contour plots of the local shift vector length $\delta = |\boldsymbol{\delta}|$ in the BLG structure, which had been twisted by $\theta = 0.4^\circ$ and sheared by $\alpha = 0.08^\circ$ along the $\beta = 0^\circ$ direction, (a) in the absence and (b) in the presence of lattice relaxation.

cept for specific values of θ, α, and β, the shear-twisted BLG (STBLG) lattice is incommensurate. For small values of θ and α, such an incommensurate structure can be approximated by a commensurate superlattice with large moiré supercells. The electronic structure of this system can be obtained to good accuracy using the continuum method described in Ref. [21].

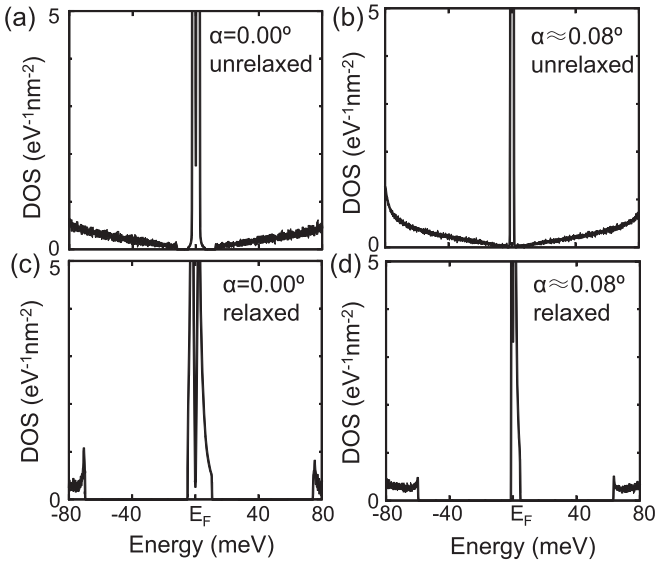

FIG. 5. Electronic density of states (DOS) in the BLG structure subject to the magic angle twist $\theta_m = 1.08^\circ$. Results for the unsheared structure are shown in (a) and (c), and those for the top layer sheared by $\alpha = 0.08^\circ$ along the $\beta = 0^\circ$ direction are shown in (b) and (d). Results for the unrelaxed structure in (a) and (b) are compared to those for the relaxed structure in (c) and (d). The energy scale is extended in comparison to Fig. 3.

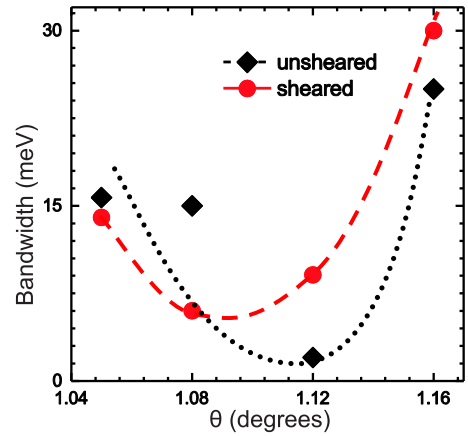

FIG. 6. The width of the flat band in a relaxed twisted bilayer graphene structure as a function of the twist angle θ. Data points for commensurate, relaxed structures in the vicinity of the observed value $\theta_m = 1.08^\circ$ are presented by the black diamonds for the unsheared lattice and by the red circles for the structure with the top layer sheared by $\alpha \approx 0.08^\circ$ along the $\beta = 0^\circ$ direction. The dotted and dashed lines are guides to the eye.

The reciprocal moiré superlattice is spanned by the two vectors $\mathbf{b}_1^{(s)} = \mathbf{b}_2 - \mathbf{b}'_2$ and $\mathbf{b}_2^{(s)} = (\mathbf{b}'_1 + \mathbf{b}'_2) - (\mathbf{b}_1 + \mathbf{b}_2)$. In our notation, $\mathbf{b}_j$, with $j = 1, 2$, are the two vectors spanning the reciprocal lattice of the bottom layer, and the primed vectors $\mathbf{b}'_j$ span the reciprocal lattice of the top layer. The two reciprocal lattice vectors $\mathbf{b}_1^{(s)}$ and $\mathbf{b}_2^{(s)}$ define the lattice vectors $\mathbf{a}_1^{(s)}$ and $\mathbf{a}_2^{(s)}$ of the direct Bravais STBLG superlattice. When $\mathbf{a}_1^{(s)}$ and $\mathbf{a}_2^{(s)}$ both belong to the Bravais lattice of the individual layers, STBLG becomes commensurate. This condition is fulfilled when $\mathbf{a}_1^{(s)} = M_1\mathbf{a}_1 + N_1\mathbf{a}_2$ and $\mathbf{a}_2^{(s)} = M_2\mathbf{a}_1 + N_2\mathbf{a}_2$, with integer values of M_1, N_1, M_2, and N_2.

The supercell area of the sheared top layer remains the same as that of the unsheared bottom layer if $M_2 + N_2 = N_1 - 1$. The quantities M_1, N_1, M_2, and N_2 uniquely define the twist angle θ, the shear angle α, and the shear direction angle β of the top layer. One geometry near the first magic angle, characterized by $(M_1, N_1) = (30, 31)$ and $(M_2, N_2) = (-31, 61)$, describes an unsheared twisted BLG layer with $\theta = 1.0845^\circ$ and $\alpha = 0^\circ$. Another similar geometry, characterized by $(M_1, N_1) = (31, 32)$ and $(M_2, N_2) = (-36, 67)$, describes a sheared twisted BLG layer with $\theta = 1.0845^\circ$, $\alpha = 0.0872^\circ$, and $\beta = -0.5423^\circ$. We determine the lattice relaxation and its effect on the electronic structure of the sheared and twisted BLG using the commensurate structures.

2. Mathematical background of the relaxation treatment in sheared and twisted bilayer graphene

BLG subject to rigid shear and twist, which is characterized by θ, α, and β, is further stabilized by atomic relaxation. In the bottom layer 1 with $\theta = \alpha = 0$, the in-plane displacement $\mathbf{u}^{(1)}(\mathbf{R})$ of an atom with respect to its initial position $\mathbf{R}$ can be represented by a Fourier expansion as

$$\mathbf{u}^{(1)}(\mathbf{R}) = \sum_j \tilde{\mathbf{u}}^{(1)}\left(\mathbf{G}_j^{(s)}\right) \sin\left(\mathbf{G}_j{}^{(s)}\cdot\mathbf{R}\right). \qquad \text{(A3)}$$

The sum extends over all vectors $\mathbf{G}_j^{(s)}$ of the reciprocal moiré superlattice of the BLG, which is spanned by $\mathbf{b}_1^{(s)}$ and $\mathbf{b}_2^{(s)}$.

In the twisted and sheared top layer 2, the in-plane displacement $\mathbf{u}^{(2)}(\mathbf{R})$ of an atom with respect to its position $\mathbf{R}$ in the unrelaxed, unsheared, but twisted layer can be expressed by

$$\mathbf{u}^{(2)}(\mathbf{R}) = \sum_j \tilde{\mathbf{u}}^{(2)}\left(\mathbf{G}_j^{(s)}\right) \sin\left(\mathbf{G}_j^{(s)} \cdot S_\alpha \mathbf{R}\right) + S_\alpha \mathbf{R} - \mathbf{R}. \quad \text{(A4)}$$

Here the direction angle β of the shear transformation, defined as S_α in Eq. (A1), has been rotated by the twist angle θ. We note that atomic displacements described by Eqs. (A3) and (A4) maintain the shape and size of the moiré supercells. In BLG subject to twist angles near $\theta_m = 1.08^\circ$, the summation in Eqs. (A3) and (A4) requires only the three shortest vectors of the reciprocal moiré superlattice, $\mathbf{G}_1^{(s)} = \mathbf{b}_1^{(s)}$, $\mathbf{G}_2^{(s)} = \mathbf{b}_2^{(s)}$, and $\mathbf{G}_3^{(s)} = -\mathbf{b}_1^{(s)} - \mathbf{b}_2^{(s)}$. In BLG subject to smaller twist angles θ around 0.4°, we include three additional vectors, $\mathbf{G}_4^{(s)} = 2\mathbf{b}_1^{(s)}$, $\mathbf{G}_5^{(s)} = 2\mathbf{b}_2^{(s)}$, and $\mathbf{G}_6^{(s)} = -2\mathbf{b}_1^{(s)} - 2\mathbf{b}_2^{(s)}$, for convergence.

Expressions for the in-plane atomic displacements $\mathbf{u}^{(n)}(\mathbf{R})$ in layers $n = 1, 2$ allow us to determine the shift vector $\boldsymbol{\delta}(\mathbf{R})$ at the position $\mathbf{R}$ by

$$\boldsymbol{\delta}(\mathbf{R}) = [\mathbf{u}^{(2)}(T_\theta \mathbf{R}) - \mathbf{u}^{(1)}(\mathbf{R})] + [T_\theta \mathbf{R} - \mathbf{R}]. \quad \text{(A5)}$$

The periodicity of $\mathbf{u}^{(1)}(\mathbf{R})$ and $\mathbf{u}^{(2)}(\mathbf{R})$ of the moiré superlattice, described by the Fourier sum in Eqs. (A3) and (A4), describes the same periodic behavior of $\boldsymbol{\delta}(\mathbf{R})$.

Similarly, the periodicity in the interlayer separation $d_0(\mathbf{R})$ can be evaluated by the Fourier sum

$$d_0(\mathbf{R}) = \langle d_0 \rangle + \Delta d_0 \sum_{j=1}^{3} \cos\left(\mathbf{G}_j^{(s)} \cdot \mathbf{R}\right). \quad \text{(A6)}$$

Here $\langle d_0 \rangle$ is the average interlayer distance, and Δd_0 describes the modulation of d_0. Since d_0 varies smoothly across the moiré supercell, an adequate description of $d_0(\mathbf{R})$ can be obtained using only the three shortest vectors $\mathbf{G}_j^{(s)}$ of the reciprocal moiré superlattice defined above for $j = 1$–3. Having specified the position dependence of the interlayer distance $d_0(\mathbf{R})$, the out-of-plane displacement $h^{(n)}$ of each individual layer n, used to evaluate E_{el} using Eq. (1), is given by

$$h^{(1)}(\mathbf{R}) = \tfrac{1}{2}[-d_0(\mathbf{R}) + 3\Delta d_0 + \langle d_0 \rangle], \quad \text{(A7)}$$

$$h^{(2)}(\mathbf{R}) = \tfrac{1}{2}[+d_0(\mathbf{R}) - 3\Delta d_0 - \langle d_0 \rangle]. \quad \text{(A8)}$$

With the Fourier expansions of the in-layer displacement $\mathbf{u}^{(n)}(\mathbf{R})$ and the interlayer distance $d_0(\mathbf{R})$, we can determine the elastic energy E_{el} of STBLG using Eq. (1).

To determine the interlayer interaction energy E_{int} specified in Eq. (2), we have to locate a proper expression for the interlayer interaction potential $V(\mathbf{R})$. Since $V(\mathbf{R})$ is periodic in STBLG, we can also express it as a Fourier expansion [11],

$$V(\mathbf{R}) = \sum_j \tilde{V}\left(\mathbf{G}_j^{(s)}\right) \cos\left(\mathbf{G}_j{}^{(s)} \cdot \mathbf{R}\right). \quad \text{(A9)}$$

The sum extends over all vectors $\mathbf{G}_j^{(s)}$ of the reciprocal moiré superlattice of the BLG. In reality, $V(\mathbf{R}) = V(\boldsymbol{\delta}(\mathbf{R}), d_0(\mathbf{R}))$ depends not on the global position $\mathbf{R}$, but rather on the quantities $\boldsymbol{\delta}$ and d_0, which show the same periodicity, as expressed in Eqs. (A5) and (A6). Using straightforward algebra, we arrive at the expression

$$V(\boldsymbol{\delta}, d_0) = V_{AA}(d_0) - 6\Delta V(d_0) + 2\Delta V(d_0) \sum_{j=1}^{3} \cos(\mathbf{G}_j \cdot \boldsymbol{\delta}), \quad \text{(A10)}$$

where the sum is limited to the smallest three vectors, $\mathbf{G}_1 = \mathbf{b}_1$, $\mathbf{G}_2 = \mathbf{b}_2$, and $\mathbf{G}_3 = -\mathbf{b}_1 - \mathbf{b}_2$, since V varies smoothly with $\boldsymbol{\delta}$.

We have used the expression $\Delta V(d_0) = (1/9)[V^{AA}(d_0) - V^{AB}(d_0)]$ for the periodic modulation of V in Eq. (A10), where $V^{AA}(d_0)$ and $V^{AB}(d_0)$ are the total energies of AA- and AB-stacked BLG per area, which both depend on the interlayer distance d_0. Furthermore, we have set $V^{AA}(d_0^{AA}) = 0$ as a reference value. Using our DFT results, we have fitted $V_{AA}(d_0)$ and $V_{AB}(d_0)$ by third-order polynomials. The expressions (in units of eV/Å^2) are $V^{AA}(d_0) = [0.113(d_0 - d_0^{AA})^2 - 0.340(d_0 - d_0^{AA})^3]/\Omega_0$ and $V_{AB}(d_0) = [-0.020 + 0.174(d_0 - d_0^{AB})^2 - 0.224(d_0 - d_0^{AB})^3]/\Omega_0$ when using d_0 (in Å) and the value $\Omega_0 = 5.24$ Å^2 for the area of the graphene unit cell.

With expressions for E_{el} and E_{int} in place, we can evaluate the total energy $E_{\text{tot}} = E_{el} + E_{\text{int}}$ for any BLG geometry. For given global shear characterized by α and β and given global twist given by θ, we can determine the atomic relaxations by globally minimizing the total energy with respect to $\tilde{\mathbf{u}}^{(n)}(\mathbf{G}^{(s)})$, Δd_0, and $\langle d_0 \rangle$.

3. Local relaxation in sheared and twisted bilayer graphene

The pattern of the local shift vectors δ depends primarily on the twist angle θ, which determines the domain size. The pattern in the BLG lattice twisted by a very small angle $\theta = 0.4^\circ$ is presented in Fig. 4. The domains of the moiré superlattice are significantly larger than in BLG with the magic twist angle $\theta_m = 1.08^\circ$ discussed earlier. The δ pattern in the larger domains is changed substantially by atomic relaxation. In particular, the domains of AB or BA stacking acquire a distinct triangular character that has been observed in dark-field TEM images [19,20].

4. Electronic structure changes in sheared and twisted bilayer graphene

The electronic density of states (DOS) in sheared and twisted BLG is shown in Fig. 5 in a larger energy window around E_F than in Fig. 3. We note that both atomic relaxation and global shear significantly modify the spectrum of the unsheared and unrelaxed lattice, shown in Fig. 5(a). Band gaps above and below the flat-band region are significant only in

the relaxed structure. Only the DOS of the sheared and relaxed structure in Fig. 5(d) displays a combination of a narrow flat band and band gaps above and below.

5. Value of the magic angle in unsheared and sheared twisted bilayer graphene

Since shear plays an important role in the relaxed twisted bilayer graphene, it is expected to affect the magic angle θ_m as well. In Fig. 6 we show the width of the narrow band around E_F as a function of the twist angle θ for both an unsheared BLG and for BLG with its top layer sheared by $\alpha \approx 0.08^\circ$ along the $\beta = 0^\circ$ direction. Only a few data points are shown since only a few commensurate structures with reasonably small unit cells exist in the narrow twist angle region shown. We notice that the (first) magic angle, associated with the narrowest bandwidth, occurs at 1.12° in the unsheared BLG and at 1.08° in the globally sheared BLG. The latter value in the sheared lattice agrees well with the observed value [5,6] $\theta_m(\text{expt}) \approx 1.08^\circ$.

[1] R. Bistritzer and A. H. MacDonald, Moiré bands in twisted double-layer graphene, Proc. Natl. Acad. Sci. U.S.A. **108**, 12233 (2011).

[2] E. Suárez Morell, J. D. Correa, P. Vargas, M. Pacheco, and Z. Barticevic, Flat bands in slightly twisted bilayer graphene: Tight-binding calculations, Phys. Rev. B **82**, 121407 (2010).

[3] J. M. B. Lopes dos Santos, N. M. R. Peres, and A. H. Castro Neto, Continuum model of the twisted graphene bilayer, Phys. Rev. B **86**, 155449 (2012).

[4] S. Fang and E. Kaxiras, Electronic structure theory of weakly interacting bilayers, Phys. Rev. B **93**, 235153 (2016).

[5] Y. Cao, V. Fatemi, A. Demir, S. Fang, S. L. Tomarken, J. Y. Luo, J. D. Sanchez-Yamagishi, K. Watanabe, T. Taniguchi, E. Kaxiras, R. C. Ashoori, and P. Jarillo-Herrero, Correlated insulator behaviour at half-filling in magic-angle graphene superlattices, Nature (London) **556**, 80 (2018).

[6] Y. Cao, V. Fatemi, S. Fang, K. Watanabe, T. Taniguchi, E. Kaxiras, and P. Jarillo-Herrero, Unconventional superconductivity in magic-angle graphene superlattices, Nature (London) **556**, 43 (2018).

[7] Y. Cao, J. Y. Luo, V. Fatemi, S. Fang, J. D. Sanchez-Yamagishi, K. Watanabe, T. Taniguchi, E. Kaxiras, and P. Jarillo-Herrero, Superlattice-Induced Insulating States and Valley-Protected Orbits in Twisted Bilayer Graphene, Phys. Rev. Lett. **117**, 116804 (2016).

[8] P. San-Jose, J. González, and F. Guinea, Non-Abelian Gauge Potentials in Graphene Bilayers, Phys. Rev. Lett. **108**, 216802 (2012).

[9] A. M. Popov, I. V. Lebedeva, A. A. Knizhnik, Y. E. Lozovik, and B. V. Potapkin, Commensurate-incommensurate phase transition in bilayer graphene, Phys. Rev. B **84**, 045404 (2011).

[10] K. Uchida, S. Furuya, J.-I. Iwata, and A. Oshiyama, Atomic corrugation and electron localization due to Moiré patterns in twisted bilayer graphenes, Phys. Rev. B **90**, 155451 (2014).

[11] S. Zhou, J. Han, S. Dai, J. Sun, and D. J. Srolovitz, van der Waals bilayer energetics: Generalized stacking-fault energy of graphene, boron nitride, and graphene/boron nitride bilayers, Phys. Rev. B **92**, 155438 (2015).

[12] M. M. van Wijk, A. Schuring, M. I. Katsnelson, and A. Fasolino, Relaxation of moiré patterns for slightly misaligned identical lattices: graphene on graphite, 2D Mater. **2**, 034010 (2015).

[13] S. Dai, Y. Xiang, and D. J. Srolovitz, Twisted bilayer graphene: Moiré with a twist, Nano Lett. **16**, 5923 (2016).

[14] S. K. Jain, V. Juričić, and G. T. Barkema, Structure of twisted and buckled bilayer graphene, 2D Mater. **4**, 015018 (2017).

[15] N. N. T. Nam and M. Koshino, Lattice relaxation and energy band modulation in twisted bilayer graphene, Phys. Rev. B **96**, 075311 (2017).

[16] K. Zhang and E. B. Tadmor, Structural and electron diffraction scaling of twisted graphene bilayers, J. Mech. Phys. Solids **112**, 225 (2018).

[17] F. Gargiulo and O. V. Yazyev, Structural and electronic transformation in low-angle twisted bilayer graphene, 2D Mater. **5**, 015019 (2018).

[18] S. Carr, D. Massatt, S. B. Torrisi, P. Cazeaux, M. Luskin, and E. Kaxiras, Relaxation and domain formation in incommensurate 2D heterostructures, arXiv:1805.06972.

[19] J. S. Alden, A. W. Tsen, P. Y. Huang, R. Hovden, L. Brown, J. Park, D. A. Muller, and P. L. McEuen, Strain solitons and topological defects in bilayer graphene, Proc. Natl. Acad. Sci. U.S.A. **110**, 11256 (2013).

[20] H. Yoo, K. Zhang, R. Engelke, P. Cazeaux, S. H. Sung, R. Hovden, A. W. Tsen, T. Taniguchi, K. Watanabe, G.-C. Yi, M. Kim, M. Luskin, E. B. Tadmor, and P. Kim, Atomic reconstruction at van der Waals interface in twisted bilayer graphene, arXiv:1804.03806.

[21] X. Lin and D. Tománek, Minimum model for the electronic structure of twisted bilayer graphene and related structures, Phys. Rev. B **98**, 081410(R) (2018).

[22] G. Kresse and J. Furthmüller, Efficient iterative schemes for *ab initio* total-energy calculations using a plane-wave basis set, Phys. Rev. B **54**, 11169 (1996).

[23] G. Kresse and J. Furthmüller, Efficiency of *ab-initio* total energy calculations for metals and semiconductors using a plane-wave basis set, Comput. Mater. Sci. **6**, 15 (1996).

[24] G. Kresse and J. Hafner, *Ab initio* molecular-dynamics simulation of the liquid-metal–amorphous-semiconductor transition in germanium, Phys. Rev. B **49**, 14251 (1994).

[25] P. E. Blöchl, Projector augmented-wave method, Phys. Rev. B **50**, 17953 (1994).

[26] G. Kresse and D. Joubert, From ultrasoft pseudopotentials to the projector augmented-wave method, Phys. Rev. B **59**, 1758 (1999).

[27] J. Klimeš, D. R. Bowler, and A. Michaelides, van der Waals density functionals applied to solids, Phys. Rev. B **83**, 195131 (2011).

[28] H. Peng, Z.-H. Yang, J. P. Perdew, and J. Sun, Versatile van der Waals Density Functional Based on a Meta-Generalized Gradient Approximation, Phys. Rev. X **6**, 041005 (2016).

[29] P. L. de Andres, F. Guinea, and M. I. Katsnelson, Bending modes, anharmonic effects, and thermal expansion coefficient in single-layer and multilayer graphene, Phys. Rev. B **86**, 144103 (2012).

[30] D. Liu, A. G. Every, and D. Tománek, Continuum approach for long-wavelength acoustic phonons in quasi-two-dimensional structures, Phys. Rev. B **94**, 165432 (2016).